Infection of the fittest: devil facial tumour disease has greatest effect on individuals with highest reproductive output

Konstans Wells[1,*], Rodrigo K. Hamede[2], Douglas H. Kerlin[1], Andrew Storfer[3], Paul A. Hohenlohe[4], Menna E. Jones[2], Hamish I. McCallum[1]

1 Environmental Futures Research Institute, Griffith University, Brisbane QLD 4111, Australia

2 School of Biological Sciences, University of Tasmania, Private Bag 55, Hobart, Tasmania 7001, Australia

3 School of Biological Sciences, Washington State University, Pullman, WA 99164-4236, USA

4 Department of Biological Sciences, University of Idaho, Moscow, ID 83844, USA

E-mail addresses (following order of authorship): k.wells@griffith.edu.au, Rodrigo.HamedeRoss@utas.edu.au, d.kerlin@griffith.edu.au, andrew.storfer@gmail.com, hohenlohe@uidaho.edu, MennaJones@utas.edu.au, h.mccallum@griffith.edu.au

***Correspondence**:

Konstans Wells, Environmental Futures Research Institute, Griffith University, Brisbane QLD 4111, Australia,

E-mail: k.wells@griffith.edu.au, Phone: +61 737357707, Fax: +61 737354209

Running head: Host fitness and transmissible cancer

Key words: Bayesian capture-recapture, tumour growth, fecundity, disease burden, individual fitness, disease risk, transmissible cancer, disease progression, pathogenesis

Type of article: Letters

Number of words in abstract: 147

Number of words in main text: 4,989

Number of references: 39

Number of tables: 0

Number of figures: 5

Abstract

Emerging infectious diseases rarely affect all members of a population equally and determining how individuals' susceptibility to infection is related to other components of their fitness is critical to understanding disease impacts at a population level and for predicting evolutionary trajectories. We introduce a novel state-space model framework to investigate survival and fecundity of Tasmanian devils (*Sarcophilus harrisii*) affected by a transmissible cancer, devil facial tumour disease. We show that those devils that become host to tumours have otherwise greater fitness, with higher survival and fecundity rates prior to disease induced death than non-host individuals that do not become infected, although high

tumour loads lead to high mortality. Our finding that individuals with the greatest reproductive value are those most affected by the cancer demonstrates the need to quantify both survival and fecundity in context of disease progression for understanding the impact of disease on wildlife populations.

INTRODUCTION

Infectious diseases rarely affect all individuals in a population equally (Grenfell *et al.* 2001; Lloyd-Smith *et al.* 2005). In many cases, it is the weakest, least fit, members of a population that are most impacted by pathogens. Low-ranking individuals or those in overcrowded aggregations have been reported to exhibit lower immune function and higher disease risk owing to a range of factors that can influence survival and fecundity (Sapolsky 2004). Conversely, dominant individuals that typically engage in mating and reproduction more frequently than subordinates, may trade off energetic investment in reproduction at the expense of immune-competence, ultimately increasing their disease risk (Sheldon & Verhulst 1996; Lee 2006; Sepil *et al.* 2013). In either case, higher infection risk is frequently reported in association with stress and immune-suppression, implying that the infection of relatively weakened individuals is common-place in disease spread and persistence (Beldomenico & Begon 2010).

Predicting the effects of infectious diseases on populations remains challenging due to the intricate interplay of demographic and epidemiological dynamics (Merler & Ajelli 2010; Peel *et al.* 2014). High disease-induced mortality, for example, does not necessarily imply decline in population growth if increased fecundity can compensate for the loss at the population-level (Wells *et al.* 2015), and/or if surviving individuals benefit from increased survival or reproductive opportunities due to decreased competition (Gaillard *et al.* 2000;

Coulson *et al.* 2004). Hence, the consequences of disease outbreaks at the population-level ultimately depend on individual fitness outcomes, that is, the relative reproductive potential of individuals that become host to the disease and non-host individuals, i.e. those individuals never affected by the disease. If, for example, a disthease mainly affects individuals that are unlikely to contribute to recruitment (e.g. post-reproductive individuals), even a highly lethal disease would have little effect on long-term population growth (see **Fig. 1**). If, however, the disease impacts those individuals most likely to contribute to recruitment then disease effects on population growth may be more substantial.

Here, we examine the fitness consequences of devil facial tumour disease (DFTD) for Tasmanian devils (*Sarcophilus harrisii*) using 10 years of mark-recapture data. DFTD is a recently emerged infectious disease caused by a clonal cancer, transmitted by direct transfer of live cancer cells when devils bite each other (Hawkins *et al.* 2006; Pearse & Swift 2006; Jones *et al.* 2008; Hamede *et al.* 2013). DFTD is mostly fatal, with large ulcerating tumours leading to metabolic starvation, overgrown oral cavities or organ failure resulting from metastasis. High contact rates among individuals, often resulting in aggressive interactions including biting, and frequency-dependent disease transmission have been expected to reduce devil populations to very low levels (Lachish *et al.* 2007; Hamede *et al.* 2009; McCallum *et al.* 2009). In contrast, precocial reproduction of devils when the cancer reduces population density and hence intraspecific competition has been suggested as an adaptive host mechanism (Jones *et al.* 2008; Lachish *et al.* 2009). However, the extent to which individuals that become host to the cancer exhibit different fitness compared to non-host individuals that never become infected, and the timing and extent of reproduction in relation to individual disease status has not been examined so far. In order to explore fitness in the context of individual and population-level disease progression we developed a novel state-space model

framework that integrates individual-based survival and fecundity in the context of disease progression and epidemiological dynamics over time.

METHODS

Study system and field data

We analysed mark-recapture data from individually marked Tasmanian devils collected between July 2006 and November 2015 from a population in western Tasmania (West Pencil Pine, 41°31 S, 145°46 E) (Hamede *et al.* 2015). Devils were captured at three month intervals (93 ± SD=18 days between capture sessions). The timing of capture sessions coincided with key reproductive stages during the annual cycle and were categorized into four seasons: 1) February/March (mating season), 2) May (small pouch young), 3) July/August (large pouch young), and 4) November (females are in late lactation with young in den). We further categorized capture sessions into three 3–4 year time periods: 1) 2006–2008, 2) 2009–2011, 3) 2012–2015. As a compromise between exploring temporal variation and model complexity, we chose these arbitrary intervals rather than fitting a continuous time function. Shifts in tumour strain frequency (Hamede *et al.* 2015) and host genes related to immune response (Epstein *et al.* 2016) could cause different DFTD effects on survival rates, but the exact timing of relevant events are unknown. We classified the reproductive status of females based on pouch appearance (Hesterman *et al.* 2008) into 6 categories: 1) immature, 2) oestrous, 3) postovulatory, 4) pouch young presence, 5) lactating, 6) regressing teats. The number of pouch young were counted if present. The size of each DFTD tumour detected was measured with callipers to the nearest 1-5 mm in three dimensions (depth measurements of tumours inside the skin were least accurate) and the per-capita tumour load (tumour volume to the nearest cm^3) was calculated. Hamede *et al.* (2015) provides further descriptions of field methods. See Supplementary Information for sample sizes.

Hierarchical model of individual fitness and disease progression

(1) Survival

We used a Bayesian hierarchical mark-recapture model, in which we integrated an incremental growth model of tumour load to project unknown disease states for all time steps when diseased individuals were likely to be alive but tumour load was not known. We use 'tumour load', the total volume of all tumours on an individual at a particular time, rather than modelling each individual tumour separately because some tumours merged together over time and not all tumours were distinguishable. We assume that tumour growth is governed by an underlying ergodic and irreversible Markov process (once diseased, individuals remain diseased until death and tumour load is assumed to continuously increase; the rare events where shrinking tumours have been observed are modelled by the Gamma process as described below). Our model resembles a continuous-time Markov chain model for discrete state variables, and we projected all data on a continuous time scale (the first day of the study set to one) in order to express the time of all events such as individual age, lifetime and the onset of tumour growth as Euclidean temporal distances.

We used the term 'host' for all individuals that were known to harbour tumours at any stage during their lifetime and the term 'non-host' for individuals never observed with tumours during their lifetime. Host individuals were classified as 'diseased' if tumour were present and as 'non-diseased' prior to the onset of tumour growth.

For each individual devil i, we noted the encounter at time t (the total number of trapping sessions being T) as a binary vector Y_i of length T with $y(i,t) = 1$ if the individual is encountered and $y(i,t) = 0$ otherwise. The capture records $y(i,t)$ are assumed to be random observations of the true presence-absence $z(i,t)$ of individual i at time t based on capture probability $p(i,t)$ with

$$y(i,t) \sim \text{Bernoulli}(z(i,t)p(i,t)) \quad (1).$$

The incompletely known individual states $z(i,t)$ were estimated based on the survival probability $\Phi(i,t)$ conditioned that individuals were alive at the previous time step $t\text{-}1$ such that:

$$z(i,t) \sim Bernoulli[\Phi(i,t)^{\delta(t)}\, z(i,t\text{-}1)\, I_{born}(i,t)\, (1 - I_{died}(i,t))] \quad (2).$$

The exponential scaling factor $\delta(t)$ accounts for unequal time intervals between capture sessions and was calculated as the ratio of the time interval between capture sessions to the average interval (93 days). The binary Boolean indicators $I_{born}(i,t)$ and $I_{died}(i,t)$ indicate whether individuals are born or have died at time step t (i.e. $I_{born}(i,t) = 1$ if already born and 0 otherwise, $I_{died}(i,t) = 1$ if already dead and 0 otherwise), derived from the Markov chains of individual states. For most individuals the year of birth was known and uncertainty of the exact birth date fell into a 20-day window around the 1st April; for the few individuals with unknown birthdates (8 out of 518), uncertainty in birthdates was assumed to cover the time window of 6 years before first capture according to assumed maximum devil lifespan. For analysis, we drew individual birthdates $\Pi(i)$ as random variables from a uniform distribution across individual uncertainty intervals; given $\Pi(i)$ and $z(i,t)$, for any time the individual age can be calculated given the underlying Markov process.

We modelled survival probability $\Phi(i,t)$ based on *logit*-link functions as

$$logit[\Phi(i,t)] = \mu_\Phi[age_{cat}(i,t), period(t)] + \beta_{sex}[sex(i)] + \beta_{host}[I_{host}(i)I_{age\geq 425d}(i,t)] + \beta_{tumour}[\omega_{cat}(i,t), period(t)] + B_T X_T(t) \quad (3).$$

Here, μ_Φ is the intercept, which we allowed to vary among different age classes and time periods. We considered individual age as a categorical variable $age_{cat}(i,t)$ with six levels: 1) 1 – 365 days, 2) 1 – 2 years, 3) 2 – 3 years, 4) 3 – 4 years, 4) 4 – 5 years, 5) > 5 years. The coefficient estimate β_{sex} captures variation in survival probability due to devil's sex. The coefficient β_{host} allows for variation in survival of mature host versus non-host individuals ≥

425 days old; we chose this threshold as this is the earliest age when individuals are expected to engage in reproduction and biting behaviour relevant for disease transmission (Jones *et al.* 2008). The coefficient β_{tumour} captures variation in survival according to individual tumour load category $\omega_{cat}(i,t)$, based on categorizing tumour load $\omega(i, t)$ (see below) into four different levels: 1) 0.0001 – 50 cm^3, 2) > 50 – 100 cm^3, 3) > 100 – 200 cm^3, 4) > 200 cm^3. X_T is a matrix of time steps (t = 1,…,T) of 4^{th} orthogonal polynomial order (for modelling non-linear relationships), B_T is a vector of coefficient estimates for the polynomial model of the time covariate.

Capture probability $p(i,t)$ was modelled with a *logit*-link functions as

$$logit[p(i,t)] = \mu_p(s) + \gamma_{infect}[I_{infect}(i,t)] + G_T X_T(t) \quad (4),$$

allowing the intercept to vary over season s, depending on whether individuals were diseased or not with DFTD at time t (as given by the Boolean indicator $I_{infect}(i,t)$), and as a polynomial function of time t of 4^{th} order with coefficients G_T.

(2) Reproduction

We estimated the reproductive state of female f at time t as $\eta_{Repro}(f, t)$, which was unknown when individuals were not captured and pouch appearance could not be classified (note that the double-index notation $i[f]$ is used to match individuals i from the overall model framework to female f). Transition probabilities between the different reproductive states r can be summarized into an $R \times R$ matrix (R=6 for the six different reproductive stages) with marginal sums of one. We accounted for a directional transition between reproductive stages, i.e. the probability to be in any reproductive stage is conditioned on the previous states such that individuals once oestrous cannot become immature again but individuals can repeatedly reproduce once matured. We modelled reproductive states for each individual and time step based on the matrix of transition probabilities $\Psi(r_{current}, r_{future}, s, j)$; Ψ was allowed to vary

among seasons *s* and for host versus non-host individuals as indexed by *j* and was conditional on the individuals' previous reproductive state (using the sum to unity constraint of the multinomial distribution):

$$\eta_{Repro}(f,t) \sim Multinomial[\Psi(\eta_{Repro}(f,t-1), R, s,j)\, z(i[f],t-1) + \Psi^{0}_{Repro}(R)\,(1 - z(i[f],t))\,(1 - I_{died}(i[f],t))] \quad (5).$$

We used indicator variables to distinguish transition probabilities when individuals are alive ($z(i[f],t)=1$) from those prior to individual birth ($z(i[f],t)=0$, $I_{died}(i[f],t)=0$) in order to enforce the constraint that unborn individuals ($I_{born}(i[f],t)=0$) are in the immature state ($\Psi^{0}_{Repro}(R)$ is a vector of length *R* with the first value set to 1 and all others to 0).

For each year *y* a female was alive (z(*i[f]*,t)=1), we calculated individual litter size $l(f,y)$ as the number of pouch young. Random state values of $l(f,y)$ were estimated based on the expected population-level probability $\pi(l,j)$ of the different litter sizes (with $l \in L$ indexing 1-4 young and $\sum_{l=1}^{L=5} \pi(l) = 1$) and conditional that an individual is expected to reproduce. We estimated $\pi(l,j)$ separately for host versus non-host individuals as indexed by *j*. The random variable $l(f,y)$ allowed us also to summarize the expected yearly population-level number of young. As part of preliminary analysis, we also allowed $\Psi(r_{current}, r_{future}, s, j)$ and $\pi(l,j)$ to vary for diseased versus non-diseased host individuals (i.e. the index *j* included an additional category conditioned on infection status); since results were similar we ignored this aspect in the final model to increase computational efficiency.

(3) Tumour incremental growth and projection

We fitted an incremental growth model to tumour load measurements $m(i,t)$ based on a logistic growth model which has been found to provide accurate fit to the growth of individual tumours (R.H. unpublished manuscript), and a Gamma process to account for random variation in each incremental growth step independent of the population-level mean

growth (Russo *et al.* 2009; Eaton & Link 2011). For this, we assumed field measures of tumour load $m(i,t)$ to be random draws from the underlying growth process over the time interval $t1$ and $t2$ between consecutive measurements such that

$$m(i,t2) = \omega(i,t1) + \iota(i,t2)\, dt(t2) + \varepsilon_\omega \quad (6).$$

Here, $\omega(i, t1)$ is the tumour load at time step $t1$, $\iota(i, t2)dt(t2)$ is the product of the daily increment $\iota(i, t2)$ and the length of the time interval dt between t1 and t2, and ε_ω is random Gaussian noise. The increment $\iota(i, t2) = (\omega(i, t2) - \omega(i, t1))/ dt(t2)$ is assumed to be a Gamma random variable $\iota(i, t2) \sim Gamma(P(i, t2), \lambda)$ with shape parameter $P(i, t2)$ and scale parameter $\lambda > 0$. The shape parameter $P(i, t2)$ is based on the expected mean daily tumour growth according to the underlying logistic growth with

$$P(i, t2) = \lambda[m(\mathrm{i}, \mathrm{t2}) - \omega(i, t1)]/ dt \quad (7)$$

and

$$m(\mathrm{i}, \mathrm{t2}) = \omega(i, t1)M_{max} / [\omega(i, t1 + [M_{max} - \omega(i, t1)]e^{-\alpha dt}] \quad (8)$$

where M_{max} is the asymptotic tumour load and α is the scale parameter of the logistic curve.

Parameter estimates from the incremental growth model (λ, α, M_{max}) enabled forward and backward projection of individual disease burden, which is a Markov process governed by the disease burden $\omega(i, t-1)$ at the previous time step and the probability density function over all possible increment values given the growth model (eqn. 6).

We used backward projection to estimate the date tumour load was at an assumed minimum mass of $\omega_{min} = 0.0001$, which we assumed to correspond to an arbitrary initial volume at the onset of tumour growth (note that we cannot further account for the true underlying biological process of latent and incubation period and the emergence of first lesions associated with tumour growth from the given data). We then projected individual tumour loads $\omega^P(i, t^P)$ according to equations 6-8. Note that the superscript '^{P}' is used to indicate

projected values rather than likelihood-based estimates from the data. We were not able to account for individual heterogeneity in growth parameters (λ, α, M_{max}) due to a lack of more detailed data; in order to realistically project individual disease burdens despite this shortcoming, we constrained logistic growth of individual tumours such that any projected value $\omega^P(i, t^P)$ was smaller than any previous data-derived estimate of disease burden and not larger than any future, data-driven estimate, i.e. $\omega(i, t < t^P) \leq \omega^P(i, t^P) \geq \omega(i, t > t^P)$.

(4) Force of infection

The individual disease state $d(i,t)$ of whether individual i is diseased at time t is another partially known binary state variable, which is known for all times individuals were captured and for projected tumour loads but unknown after the last capture for non-diseased individuals. We modelled $d(i,t)$ based on the infection probability $\Gamma(i,t)$, that is the probability that uninfected individual become infected, conditional they are alive.

$\Gamma(i,t)$ was modelled with a *logit*-link function as

$$\text{logit}[\Gamma(i,t)] = \mu_\Gamma[age_{cat}(i,t), period(t)] + \alpha_{sex}[sex(i)] + A_T X_T(t) \qquad (9).$$

Equivalent to the model for $\Phi(i,t)$, we modelled $\Gamma(i,t)$ with variation over age classes, sex and time and used the scaling factor $\delta(t)$ to take unequal time intervals into account; see **Supplementary Information**.

The model was fitted in a Bayesian framework with Markov Chain Monte Carlo (MCMC) sampling and the Gibbs Sampler in OpenBUGS 3.2.2 (Lunn *et al.* 2009). Parameter estimates were calculated as posterior modes and 95% highest posterior density credible intervals (CI) from 5,000 MCMC samples. Details of model fit and the model code are presented as **Supplementary Information**.

We calculated the force of infection *FoI(t)*, that is, the rate at which susceptible individuals acquire DFTD at each time *t*, as the population average from the infection probability $\Gamma(i,t)$.

We used the various state and indicator variables described above to calculate summary statistics at the individual (i.e. lifespan, the time until death after the onset of tumour growth or lifetime reproductive output of females) and population level (i.e. disease prevalence, proportion of individuals in different age classes in each capture session). We explored trends and seasonal effects of transmission rates (derived from prevalence estimated from all individuals and, alternatively, mature individuals only) with linear regression models in R (R Development Core Team 2016), running models for each set of MCMC samples to obtain posterior distribution of coefficient estimates.

RESULTS

Strikingly, we found that the overall fitness of host individuals was significantly higher in terms of both survival and reproduction than those of non-host individuals (devils never hosting tumours during their lifetime). The average survival rates of mature (≥ 425 days old) non-diseased host individuals was estimated to be 0.7 – 4 times higher than those of mature non-host individuals (odds ratio of 4.7 – 4.9 and CIs 3.3 – 9.0 for β_{host} for the time periods 2006 – 2008 and 2009 – 2011; odds ratio of 1.7 and CI 1.4 – 4.9 for the time period 2012 – 2015; temporal differences are only tendencies but not significant because of overlapping credible intervals; **Fig. 2**). Increased tumour loads of diseased host individuals did indeed lead to decreased survival rates, reducing survival of individuals with tumour burdens > 100 cm^3 to only 9 – 20% of that of non-diseased host individuals with similar effects over time (**Fig. 2**; β_{tumour}, odds ratios of 0.09 – 0.12, CIs: 0.07 – 0.21). Nevertheless, devils with tumours in the smallest size class had higher survival rates than those that never became infected. A larger proportion of host individuals had lifespans between 3 – 4 years

compared to non-host individuals, with 56% (CI: 53 – 59%) of hosts surviving to this age compared to only 38% (CI: 34 – 40%) of non-hosts (**Fig. 3**), most having died or dispersed as young before they could get infected.

Mature female host individuals reproduced on average 1.3 times (CI: 1.2 – 1.4) in their lifetime, while mature non-host females reproduced on average only 0.7 times (CI: 0.6 – 0.9). Moreover, host individuals tended to have larger litter sizes with a 63% (CI: 62 – 64%) chance of a litter sizes of four young opposed to only 47% (CI: 46 – 48%) chance for non-host individuals, which more often had litter sizes of two or three young only.

According to our incremental growth model, the average half-life time of tumours (i.e. the progression of individual tumour loads towards half the size of the asymptotic tumour load M_{max}) was 148 days (CI: 114 – 181 days); M_{max} was estimated as 202 cm^3 (CI: 198 – 223 cm^3) and the scale parameter of the logistic growth curve as $\alpha = 0.03$ (CI: 0.028 – 0.043, **Fig. S1**). The scale parameter of the Gamma process of incremental growth was $\lambda =$ 0.8 (CI: 0.6 – 1. 4), suggesting that growth of tumour loads was skewed towards relatively small incremental growth, and only occasionally, relatively large increments. Tracking the individual time until death of host individuals after the onset of tumour growth (i.e. a modelled time point prior to the time of first observation), we found that only 11% (CI: 7 – 15%) of individuals died within 90 days after the back-projected onset of tumour growth; at least 21% (CI: 13– 29%) of host individuals were likely to survive > 2 years with tumours (**Fig. S2**).

Population-level disease prevalence increased from the beginning until mid-term of the study (2006 – 2012), but we found no consistent trend in disease prevalence in the last time period (2013 – 2015) (**Fig. 4**). Disease prevalence and the proportion of non-host individuals did not vary across seasons but exhibited some long-term trends. The proportion

of non-host individuals decreased considerably during the first years of the study (2006 – 2011) and subsequently increased from 2011 to 2014 (**Fig. 4**).

Force of infection was highest in 2012 (posterior mode of 67%, CI 51 – 80%). Despite considerable uncertainty in these estimates as shown by large CIs (**Fig. 5**) we found a significant decrease in the force of infection after 2012 as shown by the odds ratio of the temporal effect (**Fig. S7**). At population level, the number of newly diseased individuals in different capture sessions was positively correlated with the number of diseased individuals in previous capture sessions (Spearmans' r = 0.51, CI: 0.34 – 0.65) and disease prevalence in previous capture sessions (Spearmans' r = 0.45, CI: 0.31 – 0.57). Changes in disease prevalence over time were positively correlated with the number of diseased individuals (Spearmans' r = 0.92, CI: 0.88 – 0.94) and the estimated total mass of all tumour loads at population level (Spearmans' r = 0.72, CI: 0.28 – 0.89). The force of infection divided by prevalence would estimate the transmission rate β if transmission was frequency-dependent (as previously suggested; McCallum *et al* 2009). There was inconclusive evidence that transmission rate estimates from August 2012 (peak in force of infection) until November 2015 declined by approximately 24% (CI: -13 – -29%) during the 3 years of the study with prevalence calculated for all individuals regardless of age, but this trend was not confirmed with prevalence estimates for mature individuals only. There were no clear seasonal differences in transmission rate estimates, which included much uncertainty according to large credible intervals (**Fig. S8**).

Declines in the finite population size estimates over time (**Fig. S3**) coincided with declines in the population-level total number of pouch young per year after 2010 (**Fig. S4**). Survival rates differed markedly for different age classes and over time (**Fig. S5**), as did the demographic structure of the populations (**Fig. S6**). Capture rates varied over season with 33 – 35% (both CIs: 31 – 39%) capture probability in February/March and November and 27%

(both CIs: 24 – 30%) capture probability in May and July/August. Capture probability dropped slightly during the course of the study (**Fig. S7**) and more than doubled for diseased host individuals (γ_{infect}) compared to uninfected individuals.

Overall model fit was reasonably good with a Bayesian p-value of 0.52. Model fit of the incremental growth models was less precise with a Bayesian p-value of 0.30; we attribute the lack of better fit largely to the limited data on disease progression and also large individual heterogeneity in tumour growth, for which we could not account in this study with a lack of more detailed field data. Results on the variation in survival rates for different age classes, population size estimates, and the age composition in each capture session are presented as **Supplementary Information**.

DISCUSSION

We found an unexpected and novel result - devil facial tumour disease (DFTD), a transmissible and devastating cancer, selectively impacts the otherwise most fit individuals in the population. Despite being affected by disease, host individuals (those that eventually become infected) had both higher survival and greater reproductive output than non-host individuals, in terms of both more annual breeding attempts and larger litter sizes. This challenges the conventional wisdom that infectious disease differentially affects *less fit* individuals in a population (de Castro & Bolker 2005). We emphasize that the novel insights in terms of individual fitness in relation to disease status gained in this study were only possible by analysing disease progression, survival and reproduction in an integrative model framework that accounts for the most likely disease states of individuals throughout their lifetimes.

Our finding that devils with relatively high fitness are also those most likely to become infected suggests that it is the socially dominant animals that are at highest risk of

infection and death from DFTD. These are the individuals that are likely to survive longer than the less fit mature individuals in the population, which most likely die from other causes before they are able to reproduce. This result is consistent with the finding of a previous study showing the most frequent biters (i.e., socially dominant animals) are most likely to become infected (Hamede *et al.* 2013). If infection selectively removes dominant individuals from a population, there may be important long-term consequences for the social structure and viability of the population, as well as for disease transmission. For example, culling of European badgers (*Meles meles*) disrupts social organisation and leads to increased movement of badgers and disease transmission to cattle (Donnelly *et al.* 2006). Likewise, selective animal removal through harvesting can change the demographic structure and population growth of many species (Milner *et al.* 2007).

Our results also have implications for understanding how disease-induced evolution in Tasmanian devil populations may be occurring. In particular, our model framework provides the opportunity to explore whether devils may evolve resistance to infection or rather tolerance to the impacts of infection, both being important host adaptation strategies (Råberg *et al.* 2009). Several lines of evidence provide robust support for the assertion that infected devils are under strong selective pressure. First, high mortality of adults from DFTD leads to rapid population declines (McCallum *et al.* 2009). A recent study provided evidence of substantial changes in the frequency of genes associated with immune function in devil populations that have been infected for as little as eight years (Epstein *et al.* 2016). Third, a small number of individuals are able to mount an immune response and, in some, tumours regress (Pye *et al.* 2016). In this context, the implications of our novel results, that it is that the otherwise most fit devils become infected, are intriguing. If adult devils with high fitness are those that become infected, the potential for selection for resistant animals would be limited. However, our results also demonstrate a recent decline in the force of

infection and transmission rate. This leads to the question of whether devils in this population may have developed resistance to infection. The initial increase in the force of infection from 2006 to 2012 (see Figure 5) is to be expected as the tumour increased in prevalence within the host population after disease emergence. It may also be a result of the replacement of a tetraploid tumour karyotype with a diploid karyotype which took effect from 2011 onwards (Hamede *et al.* 2015).The recent decline in the force of infection and transmission rate warrants further investigation, and could be due to a number of factors. There is evidence of selection at West Pencil Pine in chromosomal regions containing genes related to immune and cancer function (Epstein *et al.* 2016), possibly indicating evolution of resistance, as well as evidence of immune responses to DFTD resulting in tumour regressions and recovery after infection (Pye *et al.* 2016). Individual heterogeneity in devil behaviour such as physical interaction and biting is another possibility. The recent decline of the force of infection could have resulted from a reduction in the number of socially dominant devils from the population, if these are responsible for most transmission events. Group living and mating strategies can shape social contact networks among individuals that mediate parasite exchange (Liljeros *et al.* 2003; Cauchemez *et al.* 2011) and disease risk (Altizer *et al.* 2003; Drewe 2010; Kappeler *et al.* 2015). The possibility of synergistic effects between co-evolutionary dynamics of host-pathogen interactions and disease-driven changes in social structure over time necessitates caution when interpreting changes in disease transmission in context of host defence mechanisms. For future studies, it will be desirable to refine estimates of disease transmission rates that are currently blurred by large uncertainty and cannot account for individual heterogeneity in social status and behaviour due to the lack of data.

Disease tolerance might manifest in a number of ways, but one would be longer survival when carrying a tumour burden of a given size. Figure 2 shows no evidence that this has occurred, with the relationship between tumour size and mortality rate being

419 indistinguishable in the three time periods. A confounding factor, however, is the change in
420 the dominant tumour karyotype in the population from tetraploid in the early stages of the
421 epidemic to diploid karyotype during the course of the study (Hamede *et al.* 2015).
422 Unfortunately, distinguishing diploid from tetraploid karyotypes was not possible for most of
423 the individuals analyzed herein, and this information was therefore not included in our study.
424 Moreover, recent molecular evidence of a protective immune response of devils against
425 DFTD recorded from our study site (Pye *et al.* 2016) suggests that immune responses might
426 impact disease tolerance through regression of tumours. Reconciling these facts with our
427 findings of how population-level disease dynamics may change over time requires further
428 analysis of how individual-level heterogeneity in host and tumour genotypes and the
429 behaviour of adult 'hosts' and 'non-hosts' drive variation in demographic rates and infection
430 risk and how this translates into population-level pattern in disease dynamics.
431 Our estimates of the time until death following infection are longer than the 6
432 months previously reported (McCallum *et al.* 2009; Ujvari *et al.* 2016). These previous
433 estimates were for time until death after first detection of tumours. Estimation of the
434 incubation period and its frequency distribution is a challenging problem for DFTD
435 (McCallum *et al.* 2009). Our new, model-based estimation of survival time includes back-
436 projection of growth to a very small initial tumour volume. This may not estimate the actual
437 incubation period fully, but is a substantial improvement over previous approaches, which
438 have relied on anecdotal information on the appearance of tumours in captive animals which
439 had not been exposed to infection for extended periods (Pyecroft *et al.* 2007).
440 To determine whether and how disease-induced evolution within the devil
441 population and reciprocal evolution within the tumour population is occurring requires
442 further data and modelling. The modelling and analytical framework, we have presented in

this paper provides a template for performing such analysis, which should be also applicable to a wide range of other emerging infectious diseases in natural populations.

ACKNOWLEDGMENTS

The study was supported by grants from the National Science Foundation (DEB 1316549), the Australian Research Council Discovery (DP110102656) and Linkage (LP0561120) Schemes and the Save the Tasmanian Devil Appeal of the University of Tasmania. MJ was supported on an Australian Research Council Future Fellowship (FT100100250). RH is supported by an Australian Research Council DECRA Fellowship (DE170101116). We thank Forico Pty Ltd. for land access and Discovery Holiday Parks - Cradle Mountain for providing logistic support and accommodation during fieldwork. We thank Sarah Peck for veterinary support, Bobby Hua and Barbara Schönfeld for technical support. We are thankful to everyone involved in volunteer assistance during fieldwork. We thank David Sargent from Queensland College of Art, Griffith University, for preparing the illustration and Alison Peel for discussion. Field work procedures were approved by the University of Tasmania's Animal Ethics Committee (A0008588, A10296, A0011696, A0013326). We thank two anonymous reviewers and the editor for valuable contributions to the final draft.

Authorship: The project was initialized by MEJ, RKH and HIM, and RKH collected data; KW conceived and performed the analysis and wrote the first draft of the manuscript. All authors interpreted results and contributed to revisions.

Data accessibility statement: If the manuscript is accepted for publication in Ecology Letters, the data supporting the results will be archived in an appropriate public repository such as Dryad or Figshare and the data DOI will be included at the end of the article.

468

469

470 # REFERENCES

471 Altizer, S., Nunn, C.L., Thrall, P.H., Gittleman, J.L., Antonovics, J., Cunningham, A.A. *et al.*
472 (2003). Social organization and parasite risk in mammals: integrating theory and
473 empirical studies. *Annu. Rev. Ecol. Syst.*, **34**, 517–547.

474 Beldomenico, P.M. & Begon, M. (2010). Disease spread, susceptibility and infection
475 intensity: vicious circles? *Trends Ecol. Evol.*, **25**, 21-27.

476 Cauchemez, S., Bhattarai, A., Marchbanks, T.L., Fagan, R.P., Ostroff, S., Ferguson, N.M. *et*
477 *al.* (2011). Role of social networks in shaping disease transmission during a
478 community outbreak of 2009 H1N1 pandemic influenza. *Proc. Natl. Acad. Sci. U. S.*
479 *A.*, **108**, 2825–2830.

480 Coulson, T., Guinness, F., Pemberton, J. & Clutton-Brock, T. (2004). The demographic
481 consequences of releasing a population of red deer from culling. *Ecology*, **85**, 411–
482 422.

483 de Castro, F. & Bolker, B. (2005). Mechanisms of disease-induced extinction. *Ecol. Lett.*, **8**,
484 117-126.

485 Donnelly, C.A., Woodroffe, R., Cox, D.R., Bourne, F.J., Cheeseman, C.L., Clifton-Hadley,
486 R.S. *et al.* (2006). Positive and negative effects of widespread badger culling on
487 tuberculosis in cattle. *Nature*, **439**, 843-846.

488 Drewe, J.A. (2010). Who infects whom? Social networks and tuberculosis transmission in
489 wild meerkats. *Proc. Biol. Sci.*, **277**, 633-642.

490 Eaton, M.J. & Link, W.A. (2011). Estimating age from recapture data: integrating
491 incremental growth measures with ancillary data to infer age-at-length. *Ecol. Appl.*,
492 **21**, 2487–2497.

493 Epstein, B., Jones, M., Hamede, R., Hendricks, S., McCallum, H., Murchison, E.P. *et al.*
494 (2016). Rapid evolutionary response to a transmissible cancer in Tasmanian devils.
495 *Nature Communications*, **7**, 12684.
496 Gaillard, J.-M., Festa-Bianchet, M., Yoccoz, N.G., Loison, A. & Toigo, C. (2000). Temporal
497 variation in fitness components and population dynamics of large herbivores. *Annu.*
498 *Rev. Ecol. Syst.*, **31**, 367–393.
499 Grenfell, B.T., Bjørnstad, O.N. & Kappey, J. (2001). Travelling waves and spatial hierarchies
500 in measles epidemics. *Nature*, **414**, 716–723.
501 Hamede, R.K., Bashford, J., McCallum, H. & Jones, M. (2009). Contact networks in a wild
502 Tasmanian devil (*Sarcophilus harrisii*) population: using social network analysis to
503 reveal seasonal variability in social behaviour and its implications for transmission of
504 devil facial tumour disease. *Ecol. Lett.*, **12**, 1147–1157.
505 Hamede, R.K., McCallum, H. & Jones, M. (2013). Biting injuries and transmission of
506 Tasmanian devil facial tumour disease. *J. Anim. Ecol.*, **82**, 182–190.
507 Hamede, R.K., Pearse, A.-M., Swift, K., Barmuta, L.A., Murchison, E.P. & Jones, M.E.
508 (2015). Transmissible cancer in Tasmanian devils: localized lineage replacement and
509 host population response. *Proc. Biol. Sci.*, **282**, 20151468.
510 Hawkins, C.E., Baars, C., Hesterman, H., Hocking, G.J., Jones, M.E., Lazenby, B. *et al.*
511 (2006). Emerging disease and population decline of an island endemic, the Tasmanian
512 devil *Sarcophilus harrisii*. *Biol. Conserv.*, **131**, 307–324.
513 Hesterman, H., Jones, S.M. & Schwarzenberger, F. (2008). Pouch appearance is a reliable
514 indicator of the reproductive status in the Tasmanian devil and the spotted-tailed
515 quoll. *J. Zool.*, **275**, 130-138.

516 Jones, M.E., Cockburn, A., Hamede, R., Hawkins, C., Hesterman, H., Lachish, S. *et al.*
517 (2008). Life-history change in disease-ravaged Tasmanian devil populations. *Proc.*
518 *Natl. Acad. Sci. U. S. A.*, **105**, 10023–10027.
519 Kappeler, P.M., Cremer, S. & Nunn, C.L. (2015). Sociality and health: impacts of sociality
520 on disease susceptibility and transmission in animal and human societies. *Philos.*
521 *Trans. R. Soc. Lond. B Biol. Sci.*, **370**, doi: 10.1098/rstb.2014.0116.
522 Lachish, S., Jones, M. & McCallum, H. (2007). The impact of disease on the survival and
523 population growth rate of the Tasmanian devil. *J. Anim. Ecol.*, **76**, 926–936.
524 Lachish, S., McCallum, H. & Jones, M. (2009). Demography, disease and the devil: life-
525 history changes in a disease-affected population of Tasmanian devils (*Sarcophilus*
526 *harrisii*). *J. Anim. Ecol.*, **78**, 427–436.
527 Lee, K.A. (2006). Linking immune defenses and life history at the levels of the individual
528 and the species. *Integr. Comp. Biol.*, **46**, 1000–1015.
529 Liljeros, F., Edling, C.R. & Amaral, L.A.N. (2003). Sexual networks: Implications for the
530 transmission of sexually transmitted infections. *Microbes Infect.*, **5**, 189-196.
531 Lloyd-Smith, J.O., Cross, P.C., Briggs, C.J., Daugherty, M., Getz, W.M., Latto, J. *et al.*
532 (2005). Should we expect population thresholds for wildlife disease? *Trends Ecol.*
533 *Evol.*, **20**, 511–519.
534 Lunn, D., Spiegelhalter, D., Thomas, A. & Best, N. (2009). The BUGS project: evolution,
535 critique and future directions. *Stat. Med.*, **28**, 3049–3067.
536 McCallum, H., Jones, M., Hawkins, C., Hamede, R., Lachish, S., Sinn, D.L. *et al.* (2009).
537 Transmission dynamics of Tasmanian devil facial tumor disease may lead to disease-
538 induced extinction. *Ecology*, **90**, 3379–3392.
539 Merler, S. & Ajelli, M. (2010). The role of population heterogeneity and human mobility in
540 the spread of pandemic influenza. *Proc. Biol. Sci.*, **277**, 557–565.

541 Milner, J.M., Nilsen, E.B. & Andreassen, H.P. (2007). Demographic side effects of selective
542 hunting in ungulates and carnivores. *Conserv. Biol.*, **21**, 36-47.
543 Pearse, A.M. & Swift, K. (2006). Allograft theory: transmission of devil facial-tumour
544 disease. *Nature*, 439, 549-549.
545 Peel, A.J., Pulliam, J.R.C., Luis, A.D., Plowright, R.K., O'Shea, T.J., Hayman, D.T.S. *et al.*
546 (2014). The effect of seasonal birth pulses on pathogen persistence in wild mammal
547 populations. *Proc. Biol. Sci.*, **281**, 20132962.
548 Pye, R., Hamede, R., Siddle, H.V., Caldwell, A., Knowles, G.W., Swift, K. *et al.* (2016).
549 Demonstration of immune responses against devil facial tumour disease in wild
550 Tasmanian devils. *Biol. Lett.*, **12**, doi: 10.1098/rsbl.2016.0553.
551 Pyecroft, S.B., Pearse, A.M., Loh, R., Swift, K., Belov, K., Fox, N. *et al.* (2007). Towards a
552 case definition for devil facial tumour disease: what is it? *EcoHealth*, **4**, 346-351.
553 Råberg, L., Graham, A.L. & Read, A.F. (2009). Decomposing health: tolerance and
554 resistance to parasites in animals. *Philos. Trans. R. Soc. Lond. B Biol. Sci.*, **364**, 37-
555 49.
556 R Development Core Team (2016). R: A language and environment for statistical computing.
557 R Foundation for Statistical Computing Vienna, Austria.
558 Russo, T., Baldi, P., Parisi, A., Magnifico, G., Mariani, S. & Cataudella, S. (2009). Lévy
559 processes and stochastic von Bertalanffy models of growth, with application to fish
560 population analysis. *J Theor. Biol.*, **258**, 521–529.
561 Sapolsky, R.M. (2004). Social status and health in humans and other animals. *Annu. Rev.*
562 *Anthropol.*, **33**, 393–418.
563 Sepil, I., Lachish, S., Hinks, A.E. & Sheldon, B.C. (2013). MHC supertypes confer both
564 qualitative and quantitative resistance to avian malaria infections in a wild bird
565 population. *Proc. Biol. Sci.*, **280**.

566 Sheldon, B.C. & Verhulst, S. (1996). Ecological immunology: costly parasite defences and
567 trade-offs in evolutionary ecology. *Trends Ecol. Evol.*, **11**, 317–321.
568 Ujvari, B., Papenfuss, A.T. & Belov, K. (2016). Transmissible cancers in an evolutionary
569 context. *Inside the Cell*, **1**, 17–26.
570 Wells, K., Brook, B.W., Lacy, R.C., Mutze, G.J., Peacock, D.E., Sinclair, R.G. *et al.* (2015).
571 Timing and severity of immunizing diseases in rabbits is controlled by seasonal
572 matching of host and pathogen dynamics. *J. R. Soc. Interface*, **12**, 20141184.
573
574
575
576
577
578
579
580
581
582
583
584
585
586
587
588
589

590

591

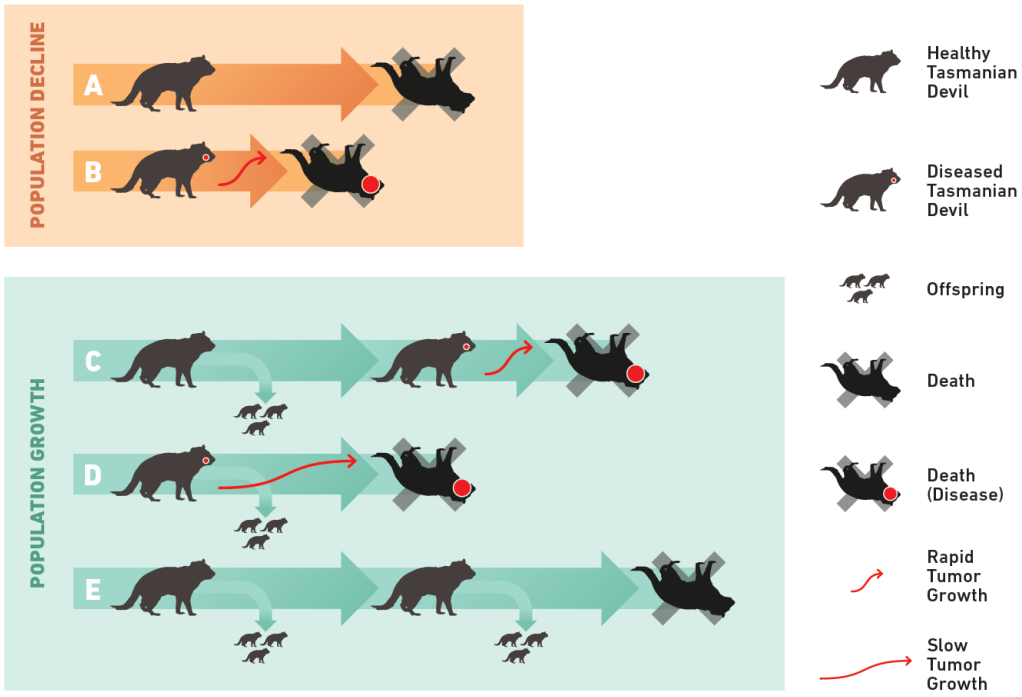

592

593 **Figure 1**. Illustration of possible synergistic effects of host survival and fecundity on long-
594 term population growth in context of disease onset and progression such as increasing tumour
595 load on Tasmanian devils. Horizontal thick lines indicate individual devil survival over time,
596 small devils reproduction and red dots infestation with tumours. Devils may not reproduce
597 because of their physical condition or social status independent of the disease (A), or, because
598 of a highly fatal disease with rapid progression and death (B), promoting population decline.
599 However, host individuals can contribute to the reproductive pool and population growth if
600 they are diseased late in life (C), or, if slow disease progression allows reproduction of
601 diseased host individuals (D). Healthy non-host individuals may reproduce several times in
602 their life (E). The outcome of these strongly coupled demographic and epidemiological
603 interactions can only be understood if analysed in a consistent framework.

604

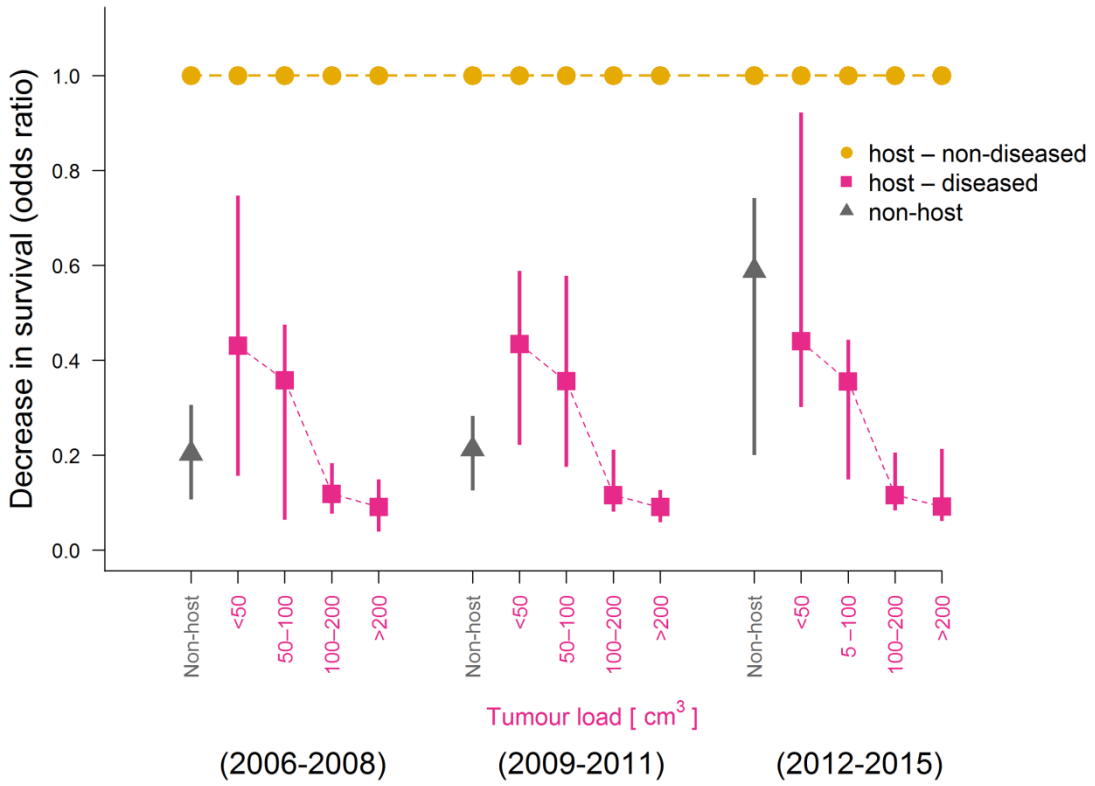

Figure 2. Estimated decrease in survival rates for mature non-host individuals (i.e. those that never become infected; grey triangles) and host individuals with certain tumour loads (red squares) compared to non-diseased host individuals (i.e. prospective host individuals prior to the onset of tumour growth). Triangles and squares are posterior modes of the odds ratios of the survival rates compared to those of non-diseased host individuals (baseline value at 1, shown in orange), vertical bars are 95% credible intervals.

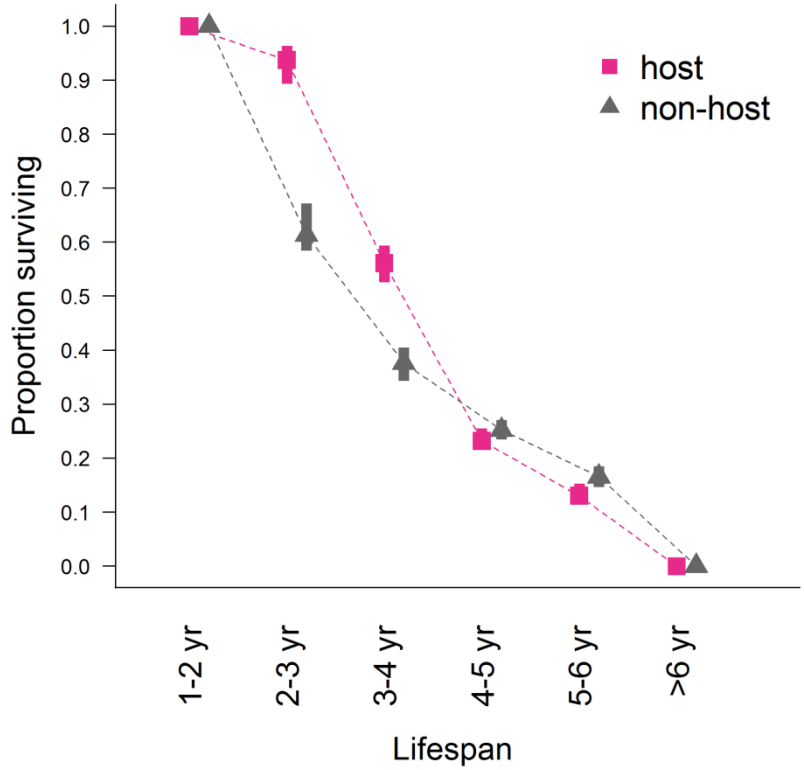

618

619 **Figure 3**. Proportion of Tasmanian devil individuals with different lifespan estimates based
620 on their classifications into host (harbour tumours at any stage during their lifetime) and non-
621 host (no tumours observed) individuals. Symbols represent the posterior mode estimates of
622 the proportion of individuals in each class of expected lifespans (1–2, 2–3, 3–4, 4–5, 5–6, > 6
623 years). Vertical bars represent 95% credible intervals based on the uncertainty in individual
624 lifespan estimates from the state-space model.

625

626

627

628

629

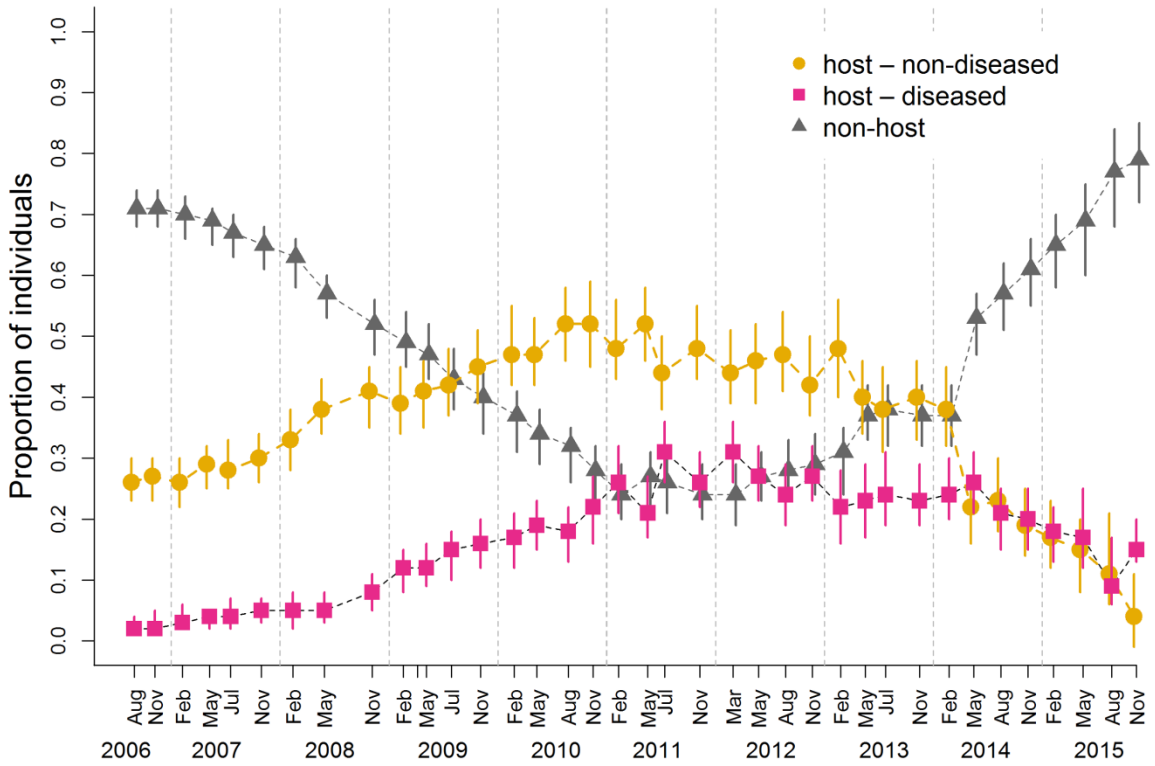

Figure 4. Changes in the proportion of individuals with different health status for devil facial tumour disease over 10 years. Disease prevalence, that is the proportion of individuals that are hosts *and* are diseased are plotted with pink circles/bars. Individuals without tumours are denoted as 'host – non-diseased' (orange circles/bars) if they were expected to acquire tumours later in their life and as 'non-host' (grey triangles/bars) if they never hosted tumours. Symbols are posterior mode estimates, bars present 95% credible intervals. For each time step, the proportions of individuals in the three different states sum to one.

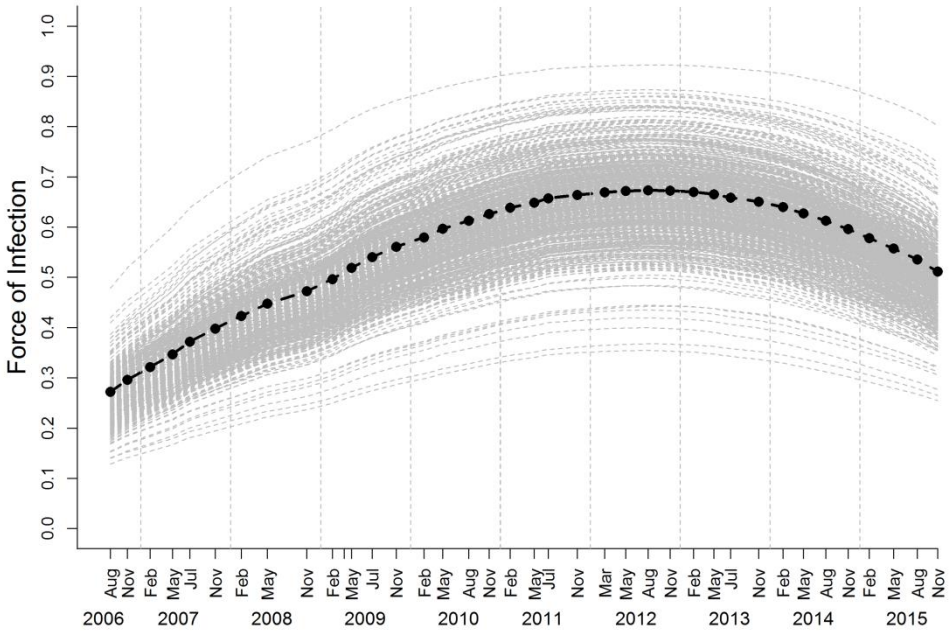

644

645 **Figure 5**. Estimated force of infection (rate at which susceptible individuals become diseased
646 per year) for devil facial tumour disease over 10 years. Black dots are posterior mode
647 estimates, bars present 95% credible intervals from sampling possible disease progression at
648 individual level.